



Temperature-based anomaly diagnosis of truss structure using Markov chain-Monte Carlo method

Jie Xu¹ · Ming Liu² · Qian Ma² · Qinghua Han¹

Received: 26 October 2021 / Revised: 28 March 2022 / Accepted: 30 March 2022 / Published online: 5 May 2022
© Springer-Verlag GmbH Germany, part of Springer Nature 2022

Abstract

Considering environmental factors such as temperature in structural health monitoring progress has been a consensus. However, the uncertainty of monitoring data usually makes it difficult. In this paper, the uncertainty factor has been introduced into the anomaly diagnosis process, a Markov chain-Monte Carlo (MCMC) anomaly diagnosis method based on temperature-induced response has been proposed. First, a novel diagnosis index has been developed based on the temperature data and static strain response data collected by the SHM system, the MCMC process is used to analyze the diagnosis index, and the posterior frequency distribution histogram of the actual diagnosis index is obtained. Finally, by analyzing the histogram of an unknown state and the initial state (baseline state) of the structure, the anomaly probability of the unknown condition is obtained, which can be used for anomaly probability diagnosis of components. The availability of the method is evaluated by a laboratory truss structure test under a series of working conditions and is verified by field monitoring data of a hanger roof structure. The results show that the method can make better use of the temperature effect of the structure for anomaly diagnosis, and the uncertainty is well considered.

Keywords Structural health monitoring · Anomaly diagnosis · Temperature-induced response · MCMC

1 Introduction

Large building structures, including truss structures, are often used in airports, stations, factories, stadiums, and other important civil infrastructures [1], such structures often encounter sudden load changes (snow loads, high wind loads), changes in restraint conditions, member damage due

to material degradation, and other structural anomalies during construction or service. Monitoring and diagnosing these structural anomalies using sensors placed on the surface of the structure is an effective means to ensure the safety of the structure throughout its life, and in recent years, with the development of sensor technology and intelligent algorithms, structural anomaly diagnosis (SAD) technique is becoming an increasingly important area.

The vibration-based method is one of the most widely used SAD methods, which reflects the abnormal state of the structure by monitoring the changes of vibration features [2–4]. However, the structural vibration features (e.g., natural frequencies) are not only related to the state of the structure itself, but also to environmental factors such as temperature, which will have an impact on the accuracy of SAD [5–7]. Although different solutions have been proposed for vibration-based SAD under environmental changes, these methods are still greatly limited by other defects in long-term practical monitoring, such as low sensitivity of vibration features to small local damage of the structure, the complicated method of sensor arrangement, and the large data transmission and storage caused by the high sampling frequency of the monitoring process, etc. [8].

✉ Qinghua Han
qhhan@tju.edu.cn

Jie Xu
jxu@tju.edu.cn

Ming Liu
ming_liu@tju.edu.cn

Qian Ma
Ma_Qian@tju.edu.cn

¹ Key Laboratory of Earthquake Engineering Simulation and Seismic Resilience of China Earthquake Administration, Key Laboratory of Coast Civil Structure Safety of Ministry of Education, School of Civil Engineering, Tianjin University, Tianjin 300350, China

² School of Civil Engineering, Tianjin University, Tianjin 300350, China

Compared to vibration monitoring data, the static responses of vital components of structures such as element stress (strain) and support displacement are sensitive to changes in the local stiffness or abnormal loads of the structure, and the utilization of these responses for SAD has received increasing attention in recent years [9, 10]. El-Sisi et al. [11] conducted static field tests of a bridge using trucks to evaluate actual strain measurements at different locations, which were used to validate the finite element model. Cocking et al. [12] arranged a health monitoring system consisting of a series of fiber optic sensors (FOS) on an inclined masonry arch railroad bridge, whose response was sensitive to passenger load, train speed, etc. Sun et al. [13] used distributed FOS to monitor the lateral buckling of rails under axial loads with different boundary conditions.

A large number of studies have shown that the static response of structures is more susceptible to environmental factors in long-term monitoring than vibration features due to the significant correlation with temperature [14]. For example, it has been found that the static strain [15], dynamic strain [16] and displacement [17] of a structure are significantly correlated with temperature. Therefore, with the periodic change of temperature, the static response also shows a periodic change [18]. Further, thermal analysis and temperature-induced stress calculation methods have been proposed [19, 20].

In recent years, there has been growing interest in SAD methods based on temperature-induced static responses (TISR), whose basic idea is that the changes in TISR in element stress or support displacement are directly related to structural stiffness or structural abnormal loads, etc. Compared with the SAD methods based on vibration or based on static response under loading, these methods directly use the TISR under ambient temperature change without additional load tests (dynamic load, static load). The benefits of these methods are their convenient sensor arrangement and low data storage, which provide a new idea for realizing long-term real-time monitoring and anomaly diagnosis of structures. Some scholars have also used some methods and techniques in TISR-based SAD, such as temperature-based structure identification [21–26], temperature-based measurement interpretation framework [27–30], ensemble empirical mode decomposition technology [31], singular spectrum analysis and the statistical control chart [32], and guided-wave based method [33]. But, most of the previous studies based on TISR have focused on bridge structures. Similar to bridge structures, there is also a significant temperature effect on the roof structures of large public buildings (e.g., planar trusses, space grid structures). Xu and Chen et al. [34, 35] conducted thirty days of monitoring during the construction of a steel roof, which found the temperature field of the structure under strong solar radiation was significant. Fan and Zhou et al. [36, 37] conducted finite element simulations

and field measurements to verify the steel roof of the Beijing Daxing International Airport terminal building. The results show that the cumulative temperature effect generated during the construction process is significant.

Therefore, the aim of the research in this paper is to propose a SAD method based on TISR applicable to truss structures. Compared with bridge structures, there are usually more members in the truss structure systems, the distribution of temperature field is complex and has a certain uncertainty [38], in addition, the noise in the SHM system will increase this uncertainty, which will have a greater impact on the SAD progress. The diagnosis indexes in most of the current SAD methods are deterministic indexes, which cannot be reasonably used to consider the uncertainty of diagnostic results caused by factors such as non-uniform temperature fields and noise. The use of uncertain diagnosis indexes based on probabilistic statistical analysis methods can be a good solution to this problem. The traditional probabilistic statistical method is based on the sample information of the structural TISR data for SAD, and the uncertainty in the sample information will have a large impact on the anomaly diagnosis [17, 39, 40].

The Bayesian method can be used to infer the posteriori information of the TISR data anomaly based on the priori and sample information. The reasons that lead to the change of the a posteriori information are mainly changes of the structure itself, which is less related to uncertainty and significantly reduces the influence of uncertainty on the SAD. However, the Bayesian method used in the current research has various problems, such as, the need for external incentives when measuring index [41]; the amount of calculation when updating parameters is large [42]; there are too many parameters that need to be estimated in the regression model [43]; the posterior distribution function of index is complicated [44, 45]; false alarms will occur when the number of index measurements is small [46–49]; the diagnosis effect is not good when the noise is high [50]; the time domain signal data volume is large that resulting in a large amount of calculation for the algorithm [51]. All the above will cause a large amount of calculation, and the timeliness of early warning for structural anomalies is a certain problem. Therefore, this paper proposes a fast SAD method, which can provide early and timely warning of possible anomalies in structural members. It also can be combined with other methods for accurate analysis and localization of structural anomalies.

In this paper, the Markov chain-Monta Carlo (MCMC) method is used in SAD based on the TISR which contains structural damage diagnosis and state change diagnosis. First, a diagnosis index that related to the physical parameters of the structure is established, which is conveniently collected from the SHM system and contains the uncertainty. Then, Considering the system uncertainty and accidental

uncertainty of the SHM system, the MCMC method is introduced to analyze the diagnosis index, and the posterior distribution is obtained. Next, an artificially determined baseline is defined, which can be considered as the state of the structure when it was just completed. Finally, Analyze the difference between the baseline state and the unknown working state, and the quantified anomaly probability of the structure is finally obtained.

2 Concept and approach

As mentioned before, the uncertainty method based on TISR is adopted to overcome the influence of uncertainty on SAD caused by temperature effects, etc. For the temperature-based anomaly diagnosis of truss structure system using the Markov chain-Monta Carlo Method proposed in this paper, the main monitoring object is the truss structure of a large public building. In this method, only the temperature and stress-induced strain are required to obtain, no additional loading or finite element model updates are required, and it is a data-driven approach to achieve SAD. The method is divided into three main phases: (1) Diagnosis index calculation; (2) Posterior distribution calculation; (3) Probabilistic anomaly diagnosis.

As shown in Fig. 1, the temperature data set and the stress-induced strain data set within a certain time series are obtained from the temperature and strain sensors arranged on the structural members, and the diagnosis index data set can be further obtained. Then, the MCMC method is used to analyze the uncertainty of the diagnosis index datasets of the structural baseline state and an unknown state, and their posterior relative frequency distributions can be obtained respectively. In the former distribution, a one-sided upper (or lower) confidence limit with a 95% guarantee is determined, and in the latter distribution, the anomaly probability of the unknown state of the structure can be determined based on the upper (or lower) confidence limit.

2.1 Diagnosis index based on T-stress-induced strain monitoring

In the SAD method of this paper, sensors need to be arranged on structural members to acquire temperature and stress-induced strain synchronously, to establish a diagnosis index based on T-stress-induced strain, which needs to directly reflect changes in the properties of structural members themselves, and thus monitor them for SAD.

Take a simply supported beam to illustrate the concept of T-stress-induced strain, which is partially constrained by a spring on the right end (length L , material thermal expansion coefficient α , elastic modulus E , spring stiffness k), as shown in Fig. 2 [14], when the temperature rises T uniformly, the

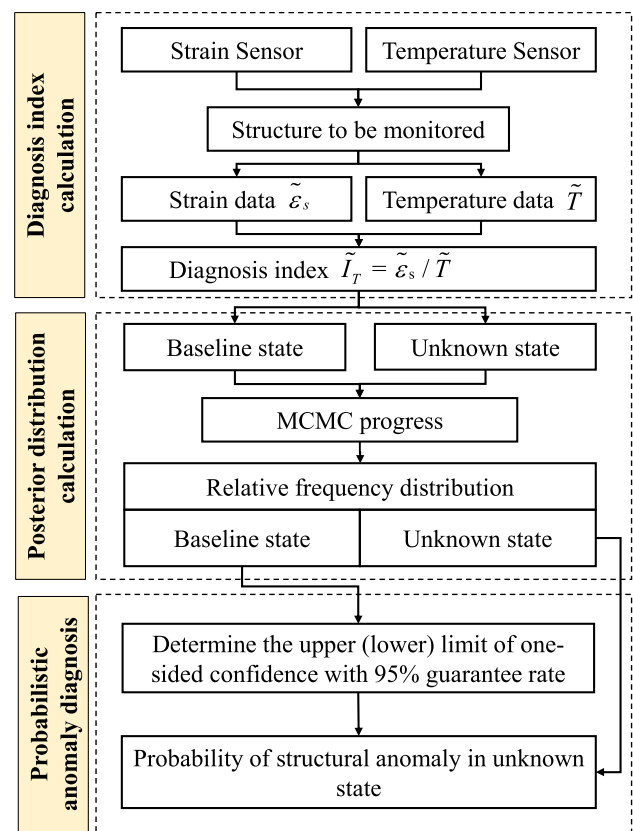


Fig. 1 The flow chart of anomaly diagnosis method

right side’s actual displacement (δ_a) can be expressed as the sum of the temperature-induced displacement (δ_t) and the stress-induced displacement (δ_s) caused by spring stress (σ):

$$\delta_a = \delta_t + \delta_s = \alpha \cdot T \cdot L + \frac{\sigma}{E} \cdot L. \tag{1}$$

The corresponding strain is

$$\epsilon_a = \epsilon_t + \epsilon_s = \alpha \cdot T + \frac{\sigma}{E}, \tag{2}$$

ϵ_s and T are stress-induced strain and temperature.

For large public building truss structures, the temperature effect is complex, there are generally different temperatures for different members, but considering that the members are generally made of metal with large thermal conductivity, and the length of the member is also small compared to the overall structure, it is considered that the temperature of each member does not change along the axial direction of the member. If it is considered that the temperature along the axis of the member changes, but in theory the member is also composed of different micro-elements in series. It is always possible to find micro-element members with uniform temperature. Therefore, the following two simplified

Fig. 2 Schematic diagram of the actual displacement and stress-induced displacement of a partially restrained beam model subject to uniform temperature change

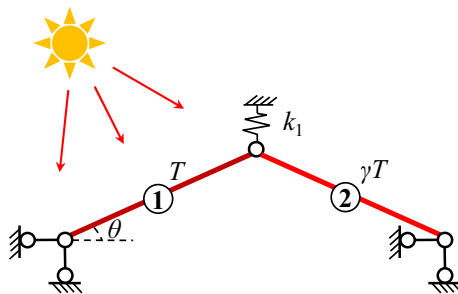
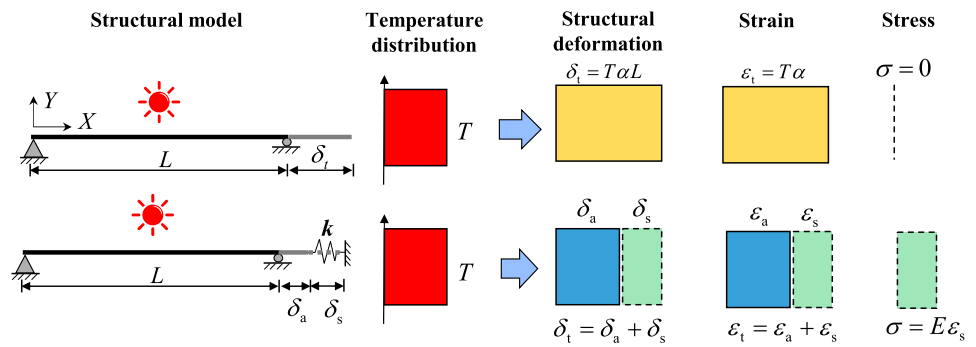


Fig. 3 The computational model of case 1 model

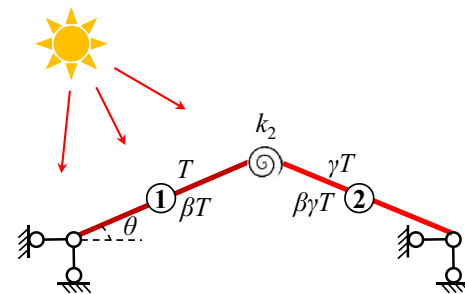


Fig. 4 The computational model of case 1

cases were selected for the derivation of the stress-induced strain [52].

(1) Case 1: different temperature for each member

As in Fig. 3, the temperature of each member is different because of sunlight, the cross-sectional area of member 1 is A_1 , the length is L , and the temperature is uniformly increased by T . The cross-sectional area of member 2 is A_2 , the length is L , and the temperature is uniformly increased by γT ($0 < \gamma < 1$). In addition, the angle between the member and the horizontal direction is θ , and the spring stiffness is k_1 . The stress-induced strain of member 1 can be found by the structural mechanics method as follows:

$$\epsilon_s = -\frac{\alpha(1 + \gamma)}{EA_1 \left(\frac{1}{EA_1} + \frac{1}{EA_2} + \frac{4 \sin^2 \theta}{k_1 L} \right)} T, \tag{3}$$

where E is the modulus of elasticity of the member material, α is the coefficient of thermal expansion of the material.

(2) Case 2: Different temperatures with gradients for each member

Due to the form of the members (hollow members) or the existence of temperature differences inside and outside the structure, there will be a temperature gradient along

the cross-sectional direction of the member. As in Fig. 4, in order to consider the temperature gradient, a rotation spring (stiffness k_2) is added to simulate the nodal rotation stiffness, and the lower surface temperature of the two members is β times the upper surface temperature ($0 < \beta < 1$), the section height of both members is h . Under the assumption that the axial deformation is much larger than the bending deformation, the stress-induced strain of member 1 can be approximated as follows:

$$\epsilon_s = -\frac{\alpha(1 + \gamma) \left(\frac{1+\beta}{2} - \frac{(1-\beta)L \tan \theta}{2h} \right)}{EA_1 \left(\frac{1}{EA_1} + \frac{1}{EA_2} + \frac{L \tan^2 \theta}{k_2} + \kappa_1 + \kappa_2 \right)} T, \tag{4}$$

where E is the modulus of elasticity of the rod material, α is the coefficient of thermal expansion of the material, κ_1, κ_2 is the bending deformation of the member 1 and 2.

$$f(\beta, L, \theta, h) = \frac{1 + \beta}{2} - \frac{(1 - \beta)L \tan \theta}{2h}, \tag{5}$$

$f(\beta, L, \theta, h)$ is a function related to the temperature gradient distribution of the members, while in practice the real temperature gradient distribution is difficult to be measured by sensors, β is constantly changing and contains uncertainty so, $f(\beta, L, \theta, h)$ can be considered as an uncertainty. One of the novelties of this paper is the consideration of this

uncertainty. If the temperature gradient is not considered, Eq. (5) will degenerate to 1.

$$\mu_c = EA_1 \left(\frac{1}{EA_1} + \frac{1}{EA_2} + \frac{L \tan^2 \theta}{k_2} + \kappa_1 + \kappa_2 \right). \tag{6}$$

Most of these structures are designed according to the spatial rod system model, so it is assumed that the bending deformation of the members is much smaller than the axial deformation, and the strain considered is also the axial strain. Therefore, the main consideration is the axial deformation $\frac{1}{EA_1} + \frac{1}{EA_2}$, while the bending deformation $\kappa_1 + \kappa_2$ can be ignored. However, it is possible that due to the existence of temperature gradient, there will be some bending deformation that cannot be accurately measured, which will cause μ_c to change as shown in Fig. 5. The consequence is to make μ_c uncertainty, which can also be considered using the method of this paper.

After the above assumptions and simplifications, and unifying the form of case 1 and case 2, the diagnosis index can be selected as Eq. (7), which is only related to the nature of the member itself and uncertainty.

$$I_T = \frac{\varepsilon_s}{T} = - \frac{\alpha(1 + \gamma)f(\beta, L, \theta, h)}{\mu_c}, \tag{7}$$

$$\mu_c = EA_1 \left(\frac{1}{EA_1} + \frac{1}{EA_2} + \frac{g(L, \theta)}{k_i} \right), \tag{8}$$

where $g(L, \theta)$ is a function related to the direction and length of the member, k_i is a parameter related to the boundary conditions.

The 3D function diagram of μ_c for different k_i ($k_{i1} > k_{i2} > k_{i3}$) values is shown in Fig. 6.

According to Fig. 6 and the above analysis, the following conclusions can be obtained:

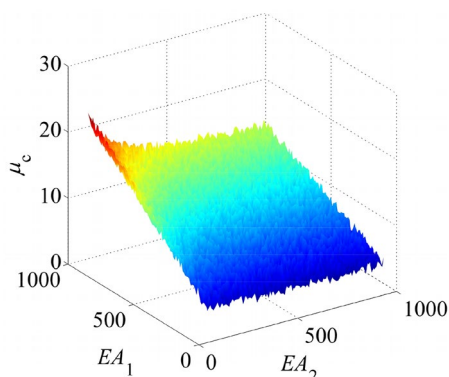


Fig. 5 Uncertainty of μ_c due to bending deformation

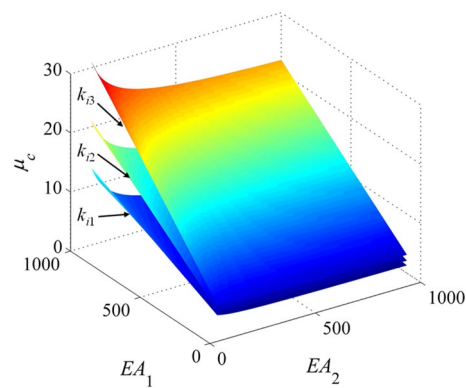


Fig. 6 3D function diagram of μ_c

There is uncertainty in the diagnosis index due to temperature gradients. The diagnosis index of the monitored member can be used to monitor not only its own anomaly but also those of its neighboring members, and is more sensitive to its own anomaly compared to its neighboring members, and its own anomaly will increase the diagnosis index, but the anomaly of its neighboring members will decrease the diagnosis index, and the index will tend to 0 as the degree of anomaly of neighboring members deepens. In addition, changes in boundary conditions can lead to changes in the diagnosis index. In fact, if the anomaly is simulated by cutting off the member in the experiment, each member can also be seen as a series connection of multiple members, and what is measured is the neighboring member of the anomaly member, which means that it will be the diagnosis index tends to 0. This is also consistent with the result that the stress-induced strain is 0 due to the free expansion of the member after cutting off. The diagnosis index can be used to effectively monitor the anomaly condition of the member where the sensor is arranged and its neighboring members.

2.2 Posterior distribution calculation based on Markov chain-Monte Carlo

In Sect. 2.1, the temperature effect of the structure is discussed to some extent, however, the real temperature field and temperature effect will be more complicated, in addition to $f(\beta, L, \theta, h)$, there is a large amount of uncertainty (e.g., noise, etc.) in the diagnosis index data set $\tilde{I}_T = \tilde{\varepsilon}_s / \tilde{T}$ obtained from the field actual measurement, and the general probabilistic statistical analysis method cannot be used to consider this kind of uncertainty well because it is based on a sample information for anomaly diagnosis. The Bayesian method is a classical method to reasonably consider such uncertainty, and the MCMC method is one of the most widespread and stable algorithms in the Bayesian method. This method of SAD using statistical probability analysis is called the uncertainty method.

The most basic principle of the Markov chain-Monte Carlo method (MCMC) comes from the Bayesian formula proposed by the British mathematician Thomas Bayes [53]. It has gradually become widely used after continuous improvement by many researchers. However, the posterior joint probability distributions of structural physical parameters are generally complex, high-dimensional, and non-standard distributions when the Bayesian formula is used in engineering practice to calculate structural physical parameters. Scholars usually use MCMC for approximation calculations, and the most widely used MCMC method is the Metropolis–Hastings (MH) algorithm [54], which is formed by the improvement and extension of the Metropolis algorithm [55].

For a certain working state M , I_T is the true value of the diagnosis index to be identified, and \tilde{I}_T is the actual measurement data set of the structural diagnosis index. Then, under the condition of known \tilde{I}_T , the posterior joint probability distribution of I_T can be obtained by the Bayesian formula:

$$p(I_T | \tilde{I}_T, M) = \frac{p(\tilde{I}_T | I_T, M)p(I_T | M)}{p(\tilde{I}_T | M)}, \tag{9}$$

where $p(\tilde{I}_T | I_T, M)$ is the probability distribution of the diagnosis index measurement data set \tilde{I}_T measured by the sensor under a certain working state M , which is a function of I_T and usually called the likelihood function of I_T ; $p(I_T | M)$ is the priori probability distribution of the parameter vector I_T , which is generally based on engineering experience and obtained from historical data; $p(\tilde{I}_T | M)$ has no relation with I_T , which is a standardized constant making the integral value of $p(\tilde{I}_T | I_T, M)$ equal to 1.

In this paper, the MH algorithm is used to calculate the above posterior distribution, a sample from the dataset \tilde{I}_T of diagnosis index measurements measured by the sensors, starting from the initial value and generating an irreducible non-periodic Markov chain according to the proposed distribution. The probability density function (PDF) curve of this Markov chain is the posterior probability distribution of the diagnosis index considering the uncertainty (as shown in Fig. 7). The process is shown in Fig. 8, and the steps are as follows.

- (1) Given the initial value $\tilde{I}_T(x_t)$ of the parameter \tilde{I}_T , the total sampling times N and set $t=0$;
- (2) Generate a candidate value $\tilde{I}_T(x')$ from the proposed distribution $g(\cdot | I_T(x_t))$;
- (3) Calculate acceptance probability

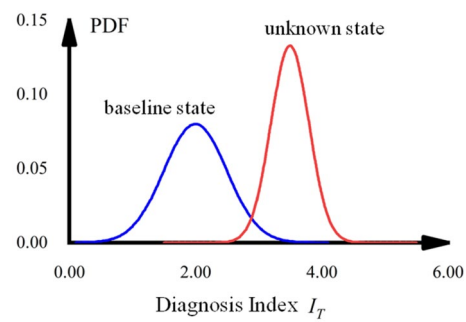


Fig. 7 Probability density function (PDF) curve of Markov chain

$$\alpha(I_T(x_t), I_T(x')) = \min \left\{ 1, \frac{I_T(x')g(I_T(x_t) | I_T(x'))}{I_T(x_t)g(I_T(x') | I_T(x_t))} \right\}. \tag{10}$$

- (4) Generate a random number u from the uniform distribution $U(0, 1)$, if $u < \alpha(I_T(x_t), I_T(x'))$, accept $I_T(x')$, let $I_T(x_{t+1}) = I_T(x')$, otherwise let $I_T(x') = I_T(x_t)$;
- (5) Let $t = t + 1$, repeat step (2)~(5), until the sampling times are reached.

2.3 Anomaly diagnosis based on relative frequency distribution histogram

For the posterior distribution of the baseline state, the 95% guaranteed upper (or lower) confidence limit is chosen because 95% confidence interval is the commonly used damage threshold interval [56, 57], as shown in Fig. 9. For the unknown states, the sum of relative frequencies greater than the upper (or less than the lower) confidence limit is determined as anomaly probability.

Further, to simplify the algorithm, the relative frequency distribution histogram is used instead of the probability density curve to calculate the anomaly probability. Next, a data set (data volume = 200) that conforms to the standard Gaussian distribution is illustrated, and the relative frequency distribution histogram of the Markov chain is shown in Fig. 10 by choosing different sampling times N for the data set by the MH algorithm. The envelope of the relative frequency distribution histogram is closer to the probability density curve of the normal distribution as the number of samples increases. According to the meaning of probability density curve and relative frequency distribution histogram, it is obvious that the relative frequency distribution histogram can be used for probability calculation instead of probability density curve.

Fig. 8 The flow chart of Metropolis–Hastings (MH) algorithm

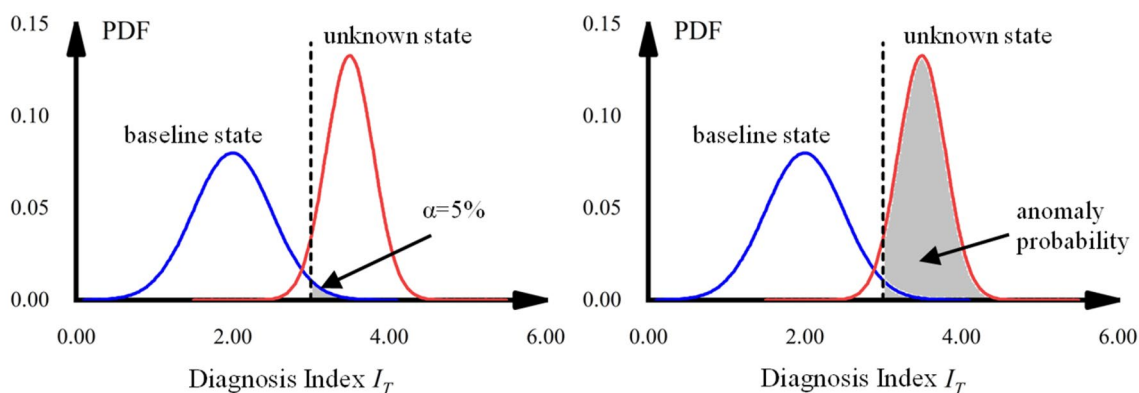
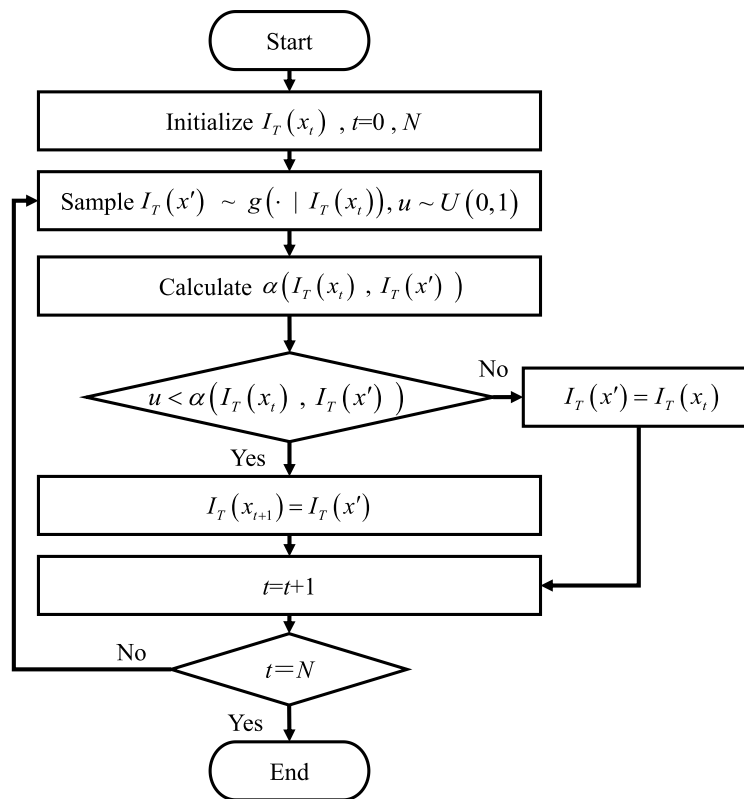


Fig. 9 Schematic diagram of anomaly probability calculation

3 Damage diagnosis test

3.1 Test overview

Damage is a type of structural anomaly, and this section seeks to validate the diagnosis method through a truss test. Therefore, in this section, the diagnosis index and the anomaly probability are referred to as the damage index and the damage probability. The planar truss shown in Fig. 11 is continuously monitored. It consists of two parts:

(1) the upper chord and web member of steel bars; (2) the lower chord of angle steel. The end of each lower chord is bolted to the steel column, the steel pile shoe is fixed in the poured concrete with four threaded rods, a certain number of weights are placed on the foot of the column to enhance the stiffness of the support and the structural integrity, and the steel bars are connected by welding, and all the members and node forms can be regarded as the types as described in Sect. 2.1

Three groups of fiber Bragg grating sensors (FBG) with temperature compensation are used to monitor the response

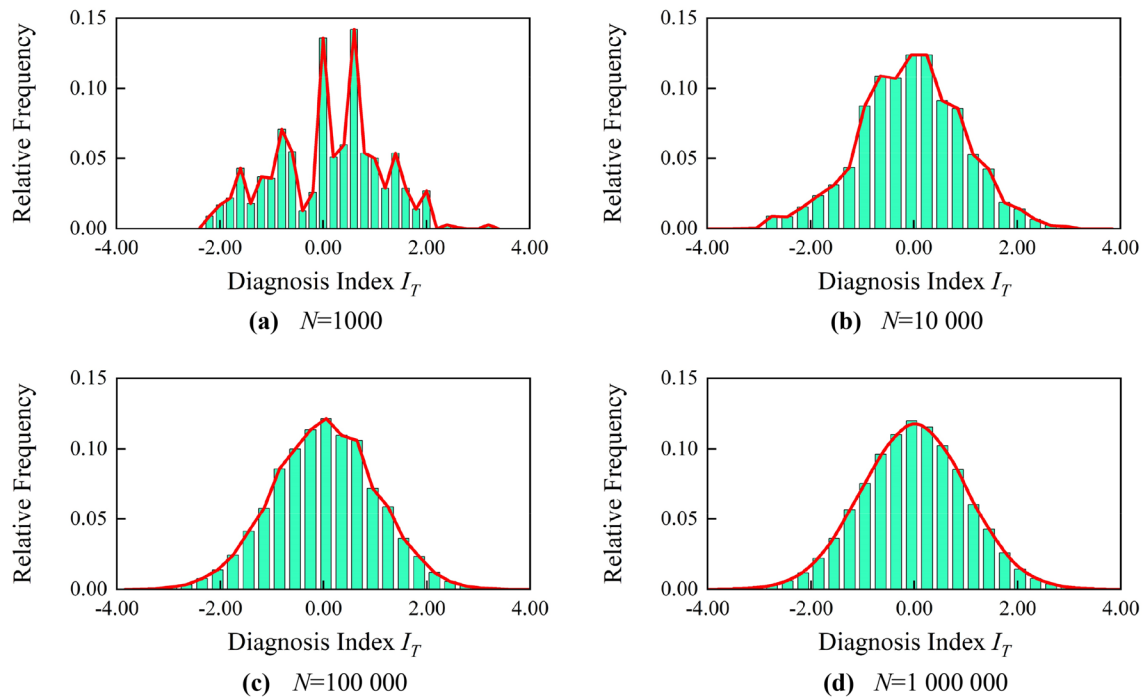


Fig. 10 Frequency distribution histogram of different sampling times

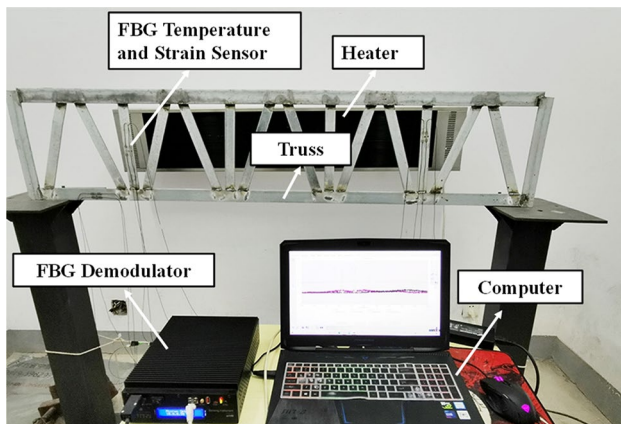


Fig. 11 A photograph of the truss test layout

of the truss. The main dimensions, geometry and sensors (S-1, S-2, S-3) arrangement of the truss are shown in Fig. 12, which also shows the members (D-1, D-2, D-3) that were damaged in order to simulate anomalies. The length of the web, diagonal and chord member are 300 mm, 335 mm and 1500 mm, respectively. Among them, the main purpose of D-1 is to study the damage of the members with sensors, and the main purpose of D-2 and D-3 is to study the damage of the neighboring members of monitored member, Damage as a cut in the member, depending on the ratio of the area of the cut section to the total section area, the degree of damage is

defined as 50% and 100%, except for baseline conditions (H, the initial non-damaged state), each damage condition (D-1, D-2, D-3) is divided into two degrees of moderate damage (50%) and complete damage (100%) (as shown in Table 1).

For FBG sensors, the principle of stress-induced strain measurement is given by Eq. (11)

$$\varepsilon_s = \frac{1}{C_2} \frac{\Delta\lambda}{\lambda} - \left(\frac{C_1}{C_2} + \alpha_{st} \right) \frac{\Delta\lambda'}{C_1 \lambda'}, \quad (11)$$

where ε_s is the strain caused by other stresses of the structure, $\Delta\lambda$, $\Delta\lambda'$ is the change in optical fiber wavelength (Strain FBG and Temperature FBG), λ , λ' is the reference wavelength of the optical fiber (Strain FBG and Temperature FBG), C_1 , C_2 are constants, α_{st} is the linear expansion coefficient of the structure.

3.2 Simulation process

Accelerated temperature cycles are simulated by adjusting the heater on and off to heat or cool the structure respectively. The purpose is to simulate the temperature cycle of the structure in the actual environment as realistically as possible in a very short time, using the heater to simulate the diurnal cycle and the natural variation of the room temperature to simulate the seasonal temperature change. A simulated diurnal cycle lasts 30 min, and five cycles are done for each working condition. Anomaly diagnosis

Fig. 12 A sketch of the truss showing its principal dimensions, locations of bolt, sensors (S-*i*, where *i* = 1, 2, 3), and the damage (D-*i*, where *i* = 1, 2, 3)

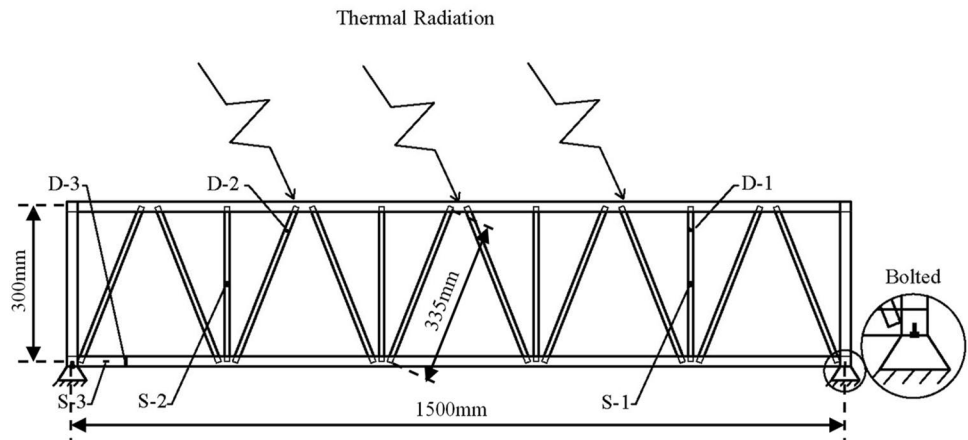


Table 1 Test conditions and sensors

Working condition	H	D-1		D-2		D-3	
Extent of damage	0%	50%	100%	50%	100%	50%	100%
Monitoring sensor	S-1, S-2, S-3	S-1, S-2, S-3		S-2, S-3		S-2, S-3	

using TISR over a smaller period is intended to be extended to the application scenario of real-time warning. In addition, in the actual detection, if TISR over a longer period is used, the data may be disturbed by many uncertainties such as seasonal trend changes, sudden temperature drops caused by rainfall, etc., resulting in uncontrollable diagnostic results. And simultaneous acquisition of $\tilde{\epsilon}_s$ and \tilde{T} with a sampling frequency of 1 Hz. The order of damage is D-1, D-2, D-3. This is because the damaged welded truss is not easily restored. The purpose of D-1's test is relatively simple (diagnose self-damage), and it is farther away from S-2, S-3, furthermore, because strain is a quantity describing local characteristics, it can minimize the influence of D-1 on the data of sensor S-2 and S-3 after the complete damage of D-1. In addition, damage D-1 (100%) and D-2 (100%) can also be used as a new baseline health condition. The temperature, strain time history curve and the strain-temperature scatter plot of the sensor S-1 in the working condition H are shown in Fig. 13. The smaller the temperature variation, the more uncertainty will be included in the strain monitoring data. Therefore, in the experimental design of this paper, the temperature is controlled in a small range (the most unfavorable temperature condition) to verify whether the method of this paper can consider this uncertainty well. The temperature and strain have a significant correlation, as shown in Fig. 13a. In addition, the measured strain data will have a high degree of uncertainty. From Fig. 13b, the strain-temperature scatter points are not on the same straight line, but present a band-like distribution, indicating that the damage index measurement data set \tilde{I}_T has a certain accidental uncertainty. And under working condition D-1 (50%), sensor S-1 has many data points in the 95% confidence interval

of H-S-1, which means that the deterministic method cannot diagnose damage well. In contrast, for Fig. 13c and d, the temperature does not show a linear correlation with the strain due to the uncertainty.

3.3 Damage diagnosis process

For different working conditions, (shown in Fig. 14), different temperature and strain data were collected, and damage index measurement sets were established.

3.3.1 Analysis of the mean value of Markov chain

The Markov chain's mean values of different working conditions and sensors obtained by MCMC sampling are shown in Table 2.

(1) Working condition D-1

There is a significant change in the data for sensor S-1. The mean value changes from -3.69 under working condition H to -2.68 under working condition D-1 (50%) and then to 0.14 under working condition D-1 (100%), while the effect on sensors S-2 and S-3 is less because the main test purpose of the damage, D-2 and D-3, is not related to sensor S-1. The mean value of sensor S-1 data becomes around 0 after this condition, so no further monitoring is performed. Although the S-3 member is a neighboring member of D-1, it is too far from the damage, so there is a large change only under the working conditions of D-1 (100%).

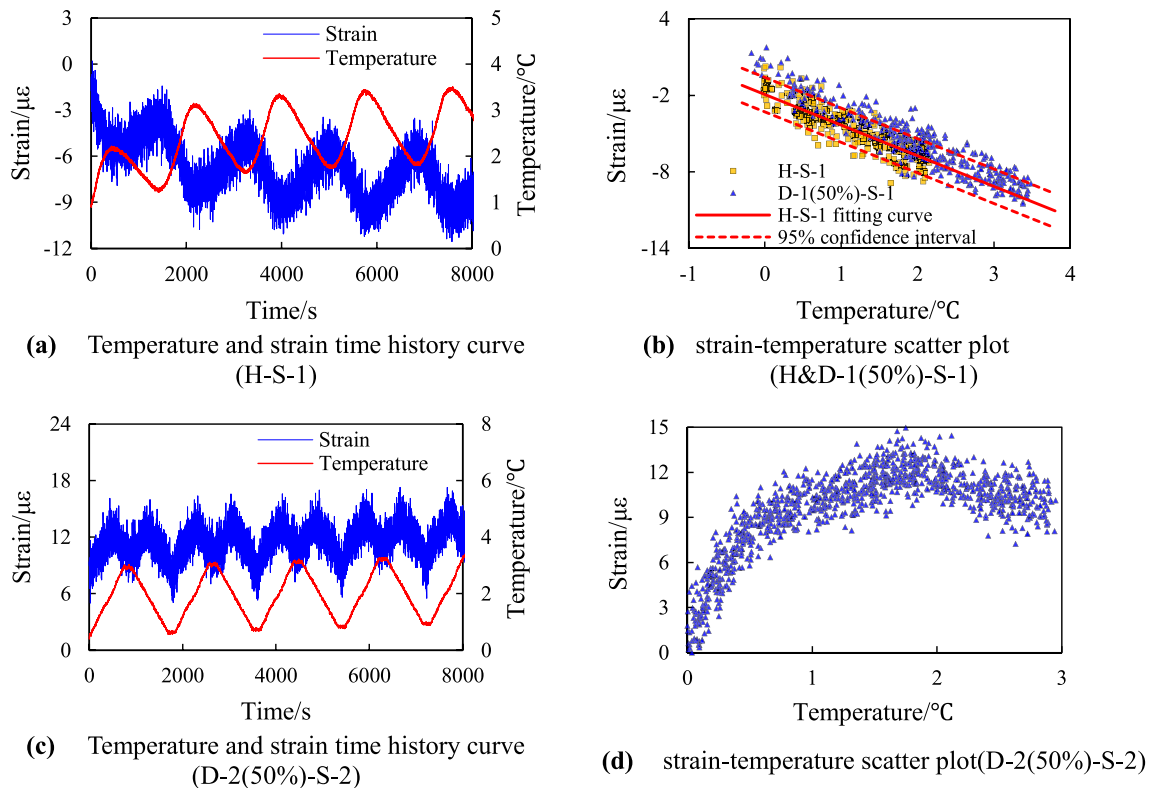


Fig. 13 Temperature and strain time history curve and strain-temperature scatter plot of sensor S-1&S-2

(2) Working condition D-2

It can be seen that the mean value of S-2 changed from -1.78 under working condition D-1 (100%) to 3.68 under working condition D-2 (50%) to -2.91 under working condition D-2 (100%), with a large variation and even a positive and negative change in sign, a possible situation due to the residual stress and deformation of the welded truss, when a moderate degree of cutting damage, the stress redistributed, causing changes in the tensile and compressive properties of the damaged member, which in turn affected the S-2 data index of the sensor. After complete cut-off, it becomes a zero-force member and the sensor S-2 data returns to the compressive state. In this working state, the sensor S-3 data still has a small change.

(3) Working condition D-3

The mean value of sensor S-2 data changes to some extent from -2.91 under working condition D-2 (100%) to -2.56 under working condition D-3 (50%) to -2.09 under working condition D-3 (100%), while from working condition D-2 (100%) to working condition D-3 (50%), the mean value of sensor S-3 data becomes approximately 0, further to working condition D-3 (100%), the mean value is still 0. This indicates that the member S-3 is very

sensitive to damage, which may be due to the member S-3 is connected to the support.

3.3.2 Analysis of damage probability

The Markov chain relative frequency distribution histograms of the damage index obtained for each sensor under different working conditions are presented in Figs. 15,16,17,18. Tables 3, 4, 5, 6 show the upper confidence limits and damage probabilities calculated from the histograms. It can be seen that the histograms are characterized by a clear normal distribution.

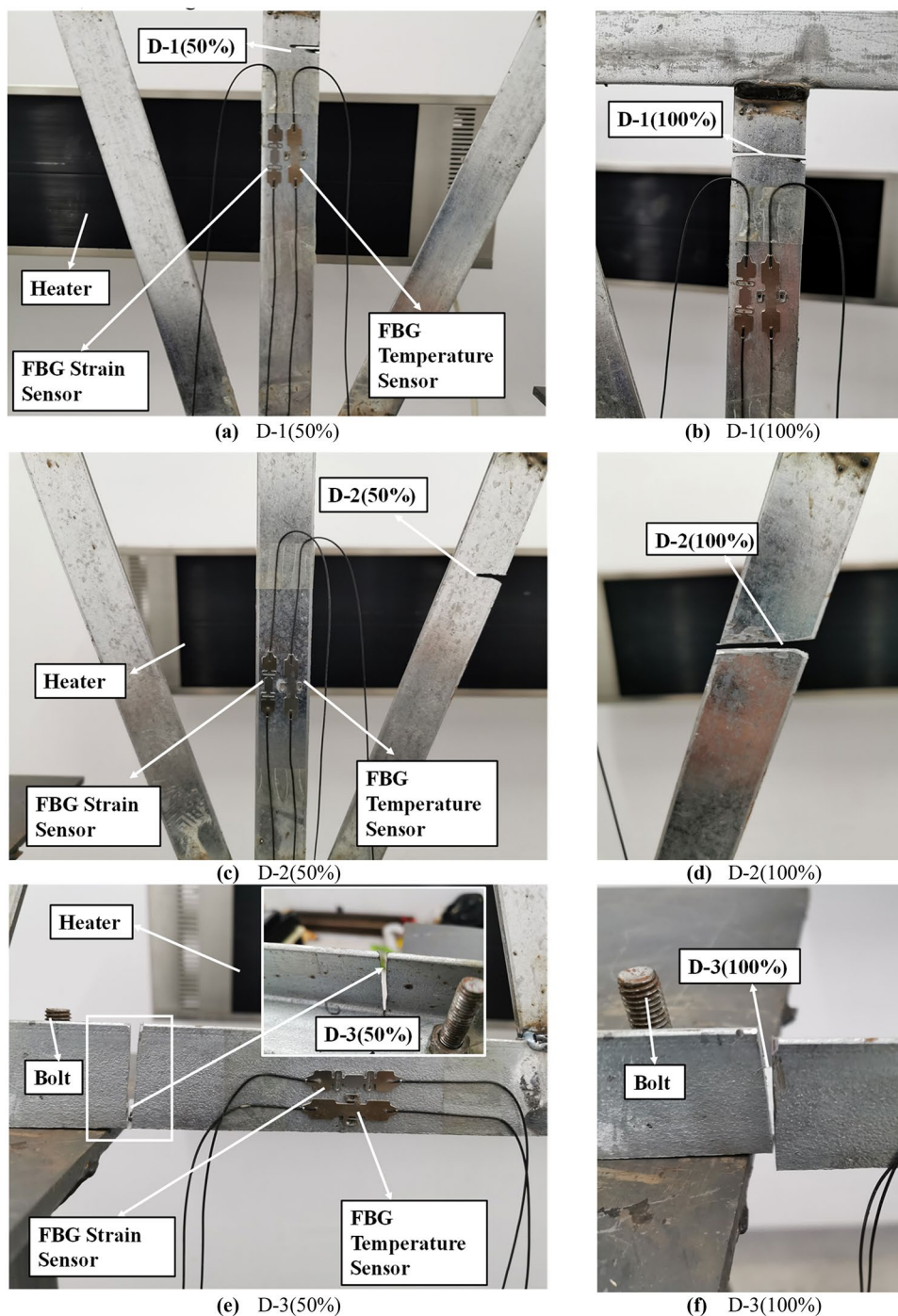
(1) Working condition H

This working condition is used as the baseline for the entire damage diagnosis method. In this test, it is considered that the members must be completely damaged. Therefore, it is only used as the diagnosis baseline for working condition D-1.

(2) Working condition D-1

Under this working condition, working condition H is used as the baseline for calculating the damage probability. It

Fig. 14 Damage and sensor details under damage condition (D-1, D-2, D-3)



can be seen that sensor S-1 can accurately diagnose the damage D-1 with a damage probability of 100.0%. Although the member S-2 is not connected to the member D-1, the index also responds to some extent. The member S-3 is connected with the member D-1, so it also has a better diagnosis effect. And working conditions with greater damage tend to have higher damage probability.

(3) Working condition D-2

Under this working condition, working condition D-1(100%) is used as the baseline for calculating the damage probability. It can be seen that sensor S-2 can accurately diagnose the damage of the member D-2, which has a common node with the member S-2, and the damage probability reaches 100.0%. As sensor S-3, although the member S-3 is connected to the member D-2, the index is not sensitive under working condition D-2(50%), but has a better diagnosis effect under more serious damage condition D-2(100%),

Table 2 Mean value of damage index Markov chain obtained by different sensors under different working conditions

Working condition and sensors	Sensors		
	S-1	S-2	S-3
H	-3.69	-1.81	-3.46
D-1(50%)	-2.68	-1.79	-3.36
D-1(100%)	0.14	-1.78	-2.98
D-2(50%)	-	3.68	-2.83
D-2(100%)	-	-2.91	-2.66
D-3(50%)	-	-2.56	0.44
D-3(100%)	-	-2.09	0.84

which may be due to the fact that member S-3 has the largest length, cross-sectional area, and is connected to the support.

(4) Working condition D-3

Under this working condition, working condition D-2(100%) is used as the baseline for calculating the damage probability. It can be seen that sensor S-2 and S-3 can accurately diagnose the damage of member D-3, which has a common node with member S-2 and S-3. This is due to the aforementioned geometric and positional particularities of member S-3, which means that its own damage has a greater impact on the whole structure.

In summary, the method has a good diagnosis effect of member damage (the monitored member itself and

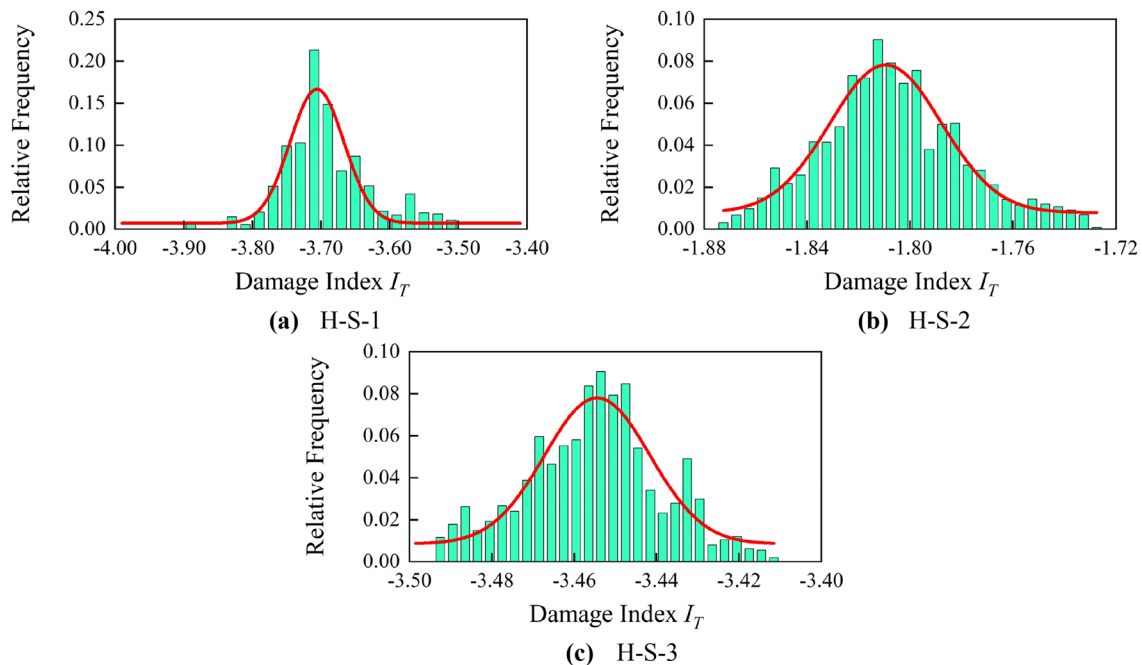
neighboring members), and can reflect the extent of damage to a certain extent.

3.3.3 Contrast with general statistical method

The main purpose of this section is to explore the effectiveness of general statistical method in this experiment.

Taking D-1(50%)-S-1 and the corresponding healthy working condition as an example, a normal distribution was fitted directly to the collected damage index data set to calculate the probability of damage. The normal distribution feature is not particularly obvious (shown in Fig. 19), and the damage probability calculated by this method is only 5.8%. In contrast, the probability of damage calculated by the MCMC method is 100%. This is because the statistical analysis based on sample information leads to inaccurate mean values of diagnosis index.

Furthermore, the sample means of the damage index measurement data sets \tilde{I}_T for different working conditions are calculated to analyze the above problem, as shown in Table 7. The mean relative deviation of the damage index dataset for the three sensors under working condition H is calculated as the theoretical value of the relative deviation. For the other working conditions, the deviation values of the mean damage index relative to working condition H were calculated separately as the actual values of relative deviations, as shown in Table 8. The trend of index and relative deviation for each sensor is shown in Fig. 20. If the actual value is less than the theoretical value, the damage

**Fig. 15** Histogram of Markov chain relative frequency distribution of damage index obtained by each sensor under working condition H

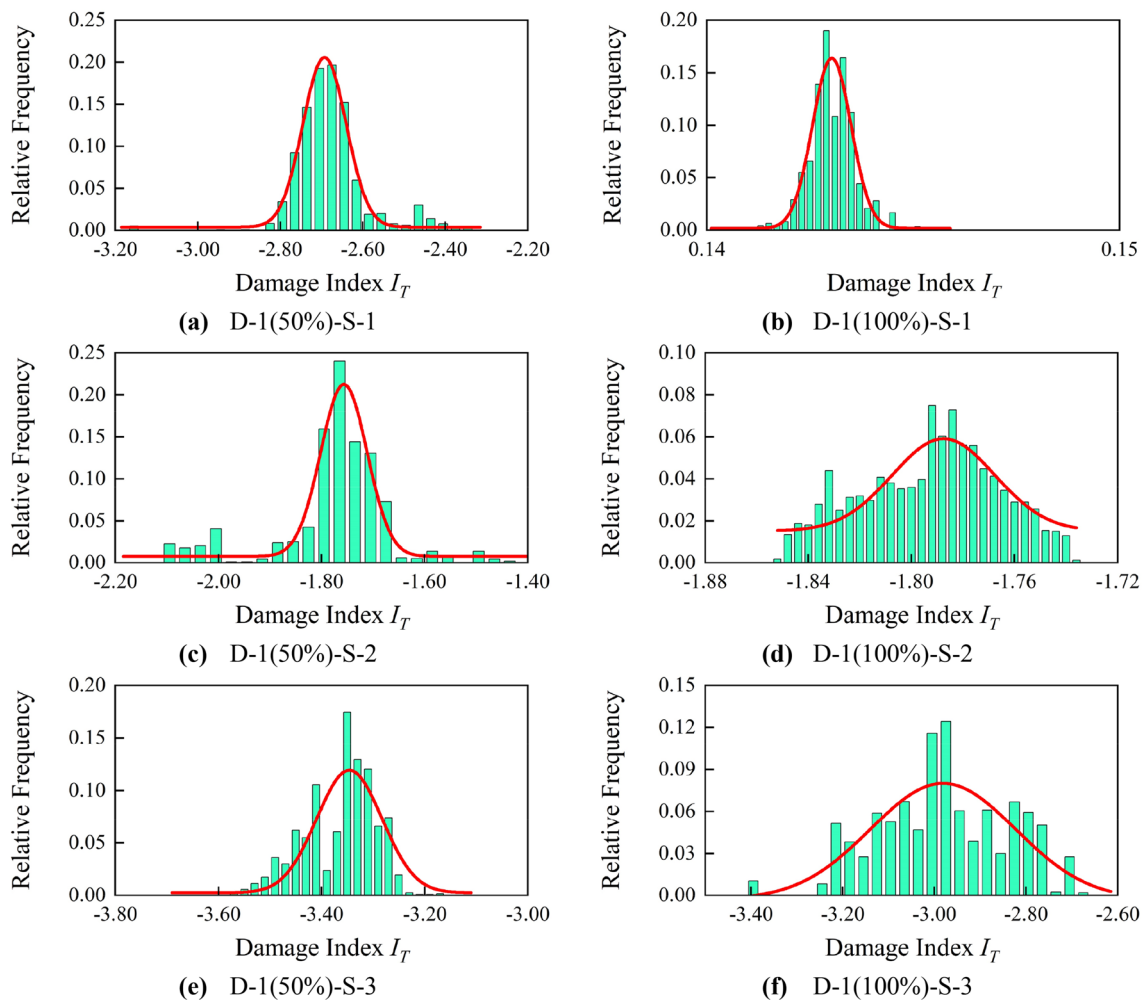


Fig. 16 Histogram of Markov chain relative frequency distribution of damage index obtained by each sensor under working condition D-1

is considered undiagnosed and submerged in uncertainty. The mean value of sensor S-1 fluctuates around 0 in the later period after the working state D-1 (100%). The sensor S-3 has a similar change after working condition D-3 (50%). As can be seen, sensor S-1 did not diagnose damage D-1 (50%), sensor S-2 did not diagnose damage D-1 (50%) and D-3 (50%), sensor S-2 did not diagnose damage D-1 (50%) and D-3 (50%), sensor S-3 did not diagnose damage D-2 (50%) and D-2 (100%). But the uncertainty methods all give a certain level of damage probability. Among them, D-1(50%)-S-1, D-3(50%)-S-3 and D-2(100%)-S-3 even reached 100.0%, D-1(50%)-S-3 also reached 82.4%.

3.3.4 Comparison with Gaussian mixture model (GMM) clustering method

However, in the actual engineering situation, it is impossible to know exactly when the structure is anomalous, which means that the collected structural response data of

an unknown state may contain data of both healthy working conditions and potential anomaly working conditions, for such scenarios, the GMM clustering method based on the Bayesian decision theory can also be used for analysis [58], in this section we mix the data of working condition H-S-1 and working condition D-1 (50%)-S-1, and GMM clustering method is performed on the above data set, and the results are shown in Fig. 21a. The clustering results are different from the real classification of the data (as shown in Fig. 21b) and cannot effectively distinguish between healthy and anomaly working conditions. Theoretically, as anomalies occur, the strain response of the same member at the same temperature will change, so the data points for different working conditions should be classified mainly according to the top and bottom, which can also be seen to be true according to the fitting curve, while the GMM clustering method obtains a left and right classification, which is mainly based on the temperature of the member, which shows that it is difficult to diagnose anomalies by

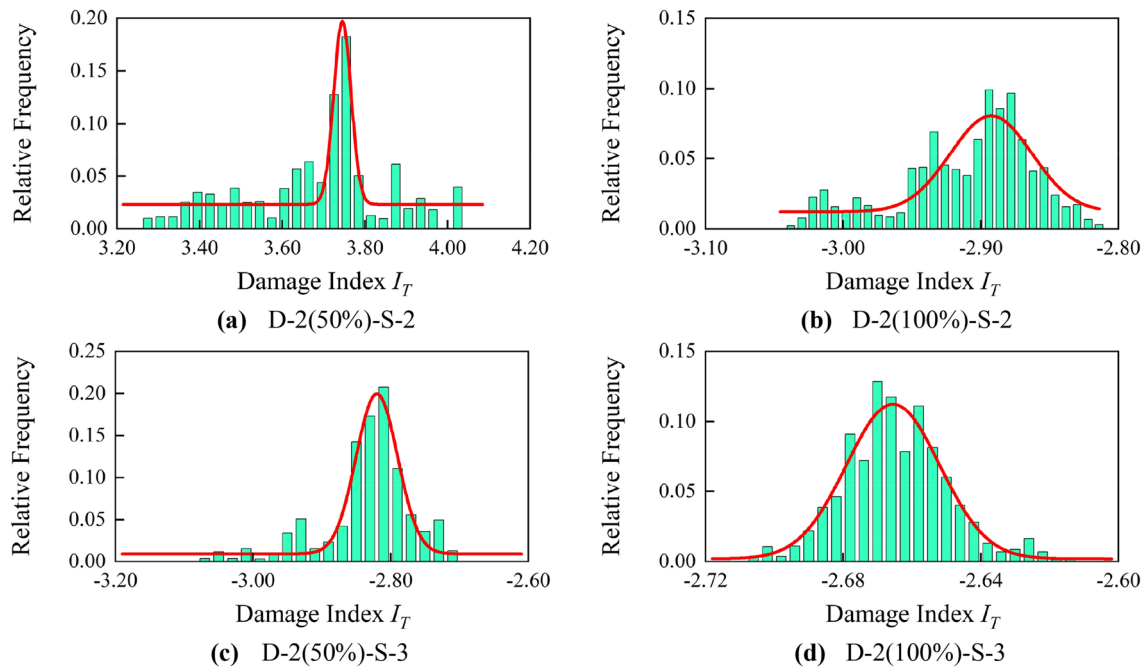


Fig. 17 Histogram of Markov chain relative frequency distribution of damage index obtained by each sensor under working condition D-2

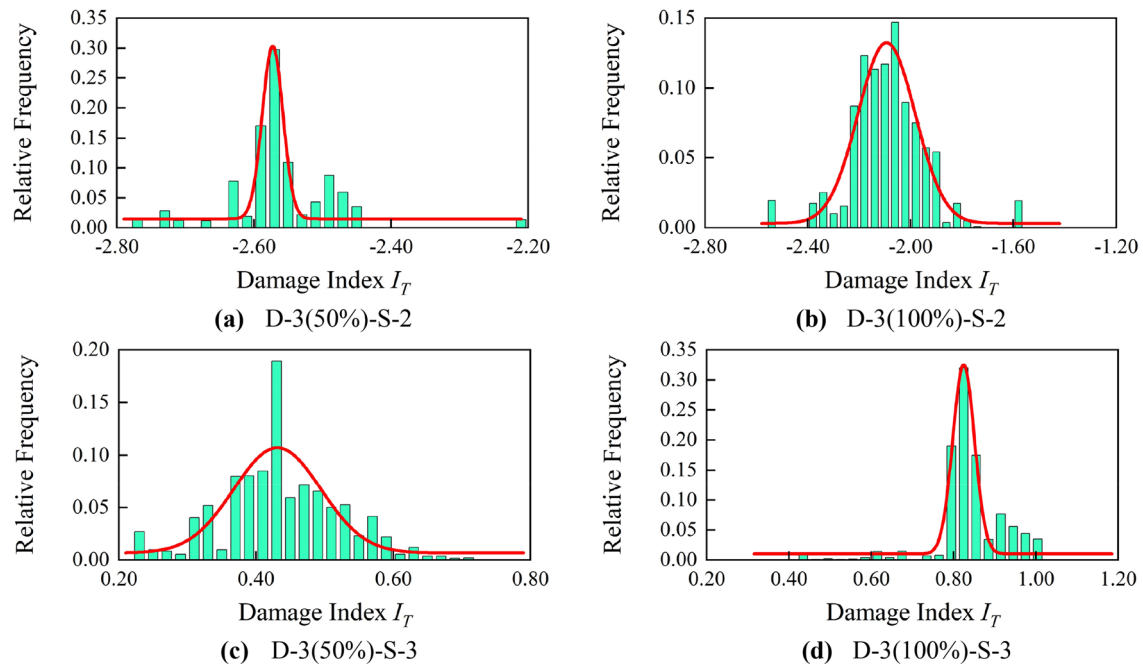


Fig. 18 Histogram of Markov chain relative frequency distribution of damage index obtained by each sensor under working condition D-3

machine learning methods without the intervention of a priori theoretical knowledge. But if the method proposed in this paper is used to diagnose anomaly in this data set, as shown in Fig. 21c, a higher anomaly probability of 74.4% can be obtained.

4 Structural state change diagnosis in site construction process

This section will attempt to investigate structural state

Table 3 Mean value of damage index Markov chain and damage probability obtained by different sensors under working condition H

Working condition and Sensors	Upper confidence limit	Damage probability
H-S-1	-3.56	-
H-S-2	-1.75	-
H-S-3	-3.43	-

Table 4 Mean value of damage index Markov chain and damage probability obtained by different sensors under working condition D-1

Working condition and sensors	Upper confidence limit	Damage probability (%)
D-1(50%)-S-1	-	100.0
D-1(100%)-S-1	-	100.0
D-1(50%)-S-2	-	7.6
D-1(100%)-S-2	-1.65	40.1
D-1(50%)-S-3	-	82.4
D-1(100%)-S-3	-2.77	100.0

Table 5 Mean value of damage index Markov chain and damage probability obtained by different sensors under working condition D-2

Working condition and sensors	Upper confidence limit	Damage probability (%)
D-2(50%)-S-2	-	100.0
D-2(100%)-S-2	-2.85	100.0
D-2(50%)-S-3	-	12.3
D-2(100%)-S-3	-2.64	100.0

Table 6 Mean value of damage index Markov chain and damage probability obtained by different sensors under working condition D-3

Working condition and sensors	Upper confidence limit	Damage probability (%)
D-3(50%)-S-2	-	100.0
D-3(100%)-S-2	-	100.0
D-3(50%)-S-3	-	100.0
D-3(100%)-S-3	-	100.0

change, another case of structural anomaly. Field monitoring data is obtained from a hangar roof structure at Beijing Daxing International Airport (BDIA). During the hangar roof structure lifting process, it may cause the boundary conditions of the structure to change, which may result in a change in the state of the structure.

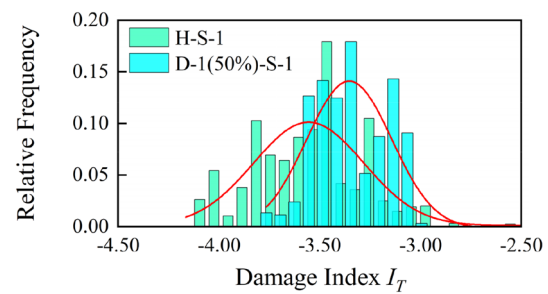


Fig. 19 Histogram of relative frequency distribution for general statistical method

Table 7 Mean value of damage index obtained by different sensors under different working conditions

Working condition and sensors	Sensors		
	S-1	S-2	S-3
H	-3.55	-2.13	-3.04
D-1(50%)	-3.34	-2.33	-4.72
D-1(100%)	0.03	-0.59	-1.95
D-2(50%)	0.14	6.01	-3.62
D-2(100%)	-0.20	-0.39	-2.73
D-3(50%)	-0.23	-2.38	0.96
D-3(100%)	-0.05	-1.63	1.09

4.1 Hangar roof structure at Beijing Daxing International Airport

The roof of the hangar hall is composed of a plane truss system and single-layer diagonal square pyramid grids, all of which are spherical tube structures, and the joints are welded spherical joints (shown in Fig. 22a). Figure 22b shows the truss system consists of four 45-degree diagonal trusses, gate trusses, and longitudinal trusses. The vibrating wire strain sensors with temperature compensation are arranged on the important members to ensure its safety during construction and operation (shown in Fig. 22c, d). A sensor is arranged on the upper and lower surface of the lower chord of DT1 ~ DT4 respectively, total 8 sensors.

During the construction process, the roof was lifted in two overall steps. The first lift of the entire grid was from August 18 to August 20, 2018. After the first lift was completed, the second lift grid was assembled and combined with the first lift grid, the second lift was completed from August 31 to September 2.

4.2 Baseline state selection

During the construction and service process of the structure, the state is constantly changing, so it is necessary to select the baseline state reasonably. The data time series of the

Table 8 Actual and theoretical relative deviation of damage index obtained by different sensors under different working conditions

Working condition and sensors	Sensors					
	S-1		S-2		S-3	
	Actual value (%)	Theoretical value (%)	Actual value (%)	Theoretical value (%)	Actual value (%)	Theoretical value (%)
H	–	18.5	–	18.8	–	21.1
D-1(50%)	5.92		9.39		55.3	
D-1(100%)	100.8		72.3		35.9	
D-2(50%)	103.9		382.2		19.1	
D-2(100%)	94.4		81.7		10.2	
D-3(50%)	93.5		11.7		131.6	
D-3(100%)	98.6		23.5		135.9	

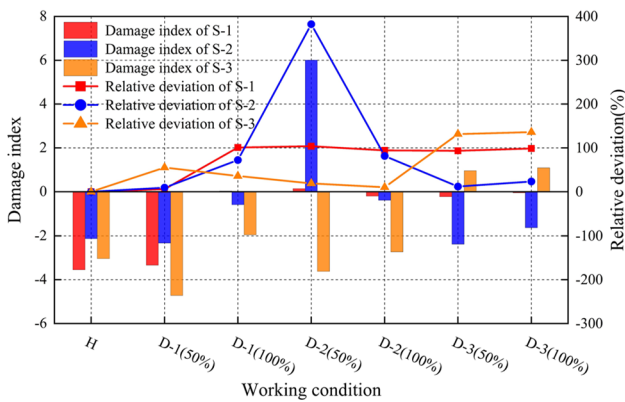


Fig. 20 Mean value of damage index and relative deviation of different sensors under different working conditions

baseline state should be stationary. In this section, the Augmented Dickey-Fuller test (ADF) is used to ensure that the selected state is stationary [59]. ADF is a type of unit root test called statistical test, which is used to check stationarity.

The null hypothesis, alternative hypothesis of the corresponding unit root test and test statistics τ are:

$$H_0 : \rho = 1, H_1 : \rho < 1$$

$$\tau = \hat{\rho}(s(\hat{\rho}))^{-1}, \tag{12}$$

where $\hat{\rho}$, $s(\hat{\rho})$ is the least squares estimate of the Autoregressive model parameters and the standard deviation of the corresponding estimate. If the test statistic is less than the critical value, we can reject the null hypothesis and say that the series is stationary.

Take member DT4-upper as an example. ADF test was performed on the diagnosis index data after the first lift and before the second lift to check the stationarity. The relevant parameters are shown in Table 9. The test statistic is less than the critical value, so the series can be considered stationary and can be selected as the baseline state.

4.3 State change diagnosis

After August 20, when the first lift ends, and before the second lift starts on August 31, a new baseline state should be selected to monitor the second lift. During this period, there are some sensor data changes are more obvious, using a simple method that is possible to make a judgment on its state, cannot highlight the superiority of the method in this paper, so this paper selects DT4-upper (The least significant change in data) as the object of analysis. The time history curves of strain and temperature are shown in Fig. 23, noted that the strain data therein were normalized relative to 8/27 for a clearer representation. For member DT4-upper, the time history curve does not change significantly and needs further analysis. The diagnosis index data from August 20 to August 31 can satisfy the ADF test, and it is selected as the baseline state for the unknown state data from August 31 to September 3. The histogram of the posterior relative frequency distribution is shown in Fig. 24, and the mean value of the Markov chain in the baseline state is -8.25 , and the mean value of the Markov chain in the unknown state is -8.69 . Because -8.25 is greater than -8.69 , the lower confidence limit should be selected as -8.64 , and the anomaly probability is 42.0%. The state change of the structure is effectively diagnosed.

5 Summary and conclusions

In this paper, a temperature-based anomaly diagnosis of truss structure system using Markov chain-Monte Carlo method is proposed, which not only introduces the uncertainty method into a SAD method based on static response monitoring, but also actively uses the temperature effect of the structure for SAD. In this method, a novel diagnosis index based on T-stress-induced strain that takes uncertainties into account is proposed, which is obtained from the stress-induced strain and temperature measured by sensors

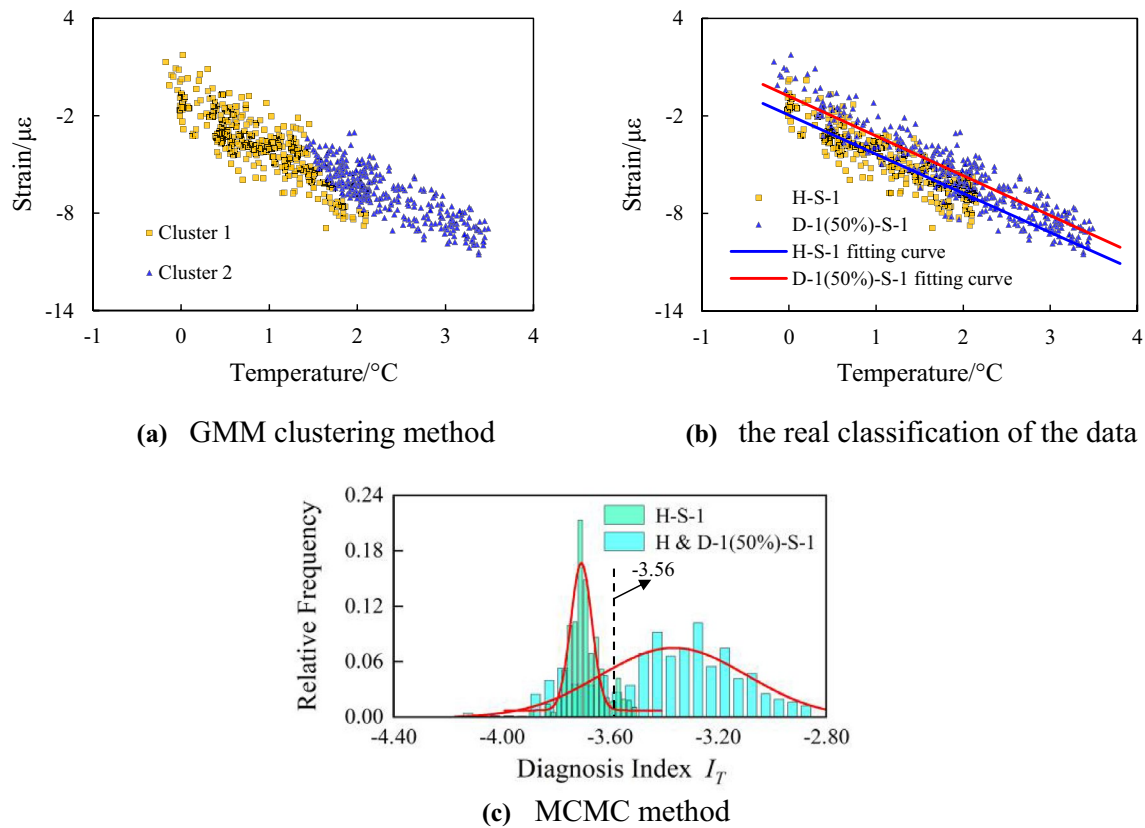


Fig. 21 Comparison of GMM clustering method and MCMC method

arranged in the focus area of the structure. Then, the diagnosis index measurement data set is processed by MCMC to obtain the posterior relative frequency distribution histogram of the actual diagnosis index, and the histogram of the baseline state and an unknown state are analyzed to obtain the structural anomaly probability of the members under this unknown state. As two aspects of anomaly diagnosis, the structural damage diagnosis and state change diagnosis were verified by a truss test and field monitoring data of the BDIA hanger roof structure respectively, and the following conclusions were obtained:

- (1) With certain simplifications and assumptions about the real temperature effects and structural forms, the derived diagnosis index can well achieve the objectives of the SAD method, which can reflect the anomalies of the member itself, the neighboring members and boundary conditions, also include the uncertainties caused by temperature effects to a certain extent.
- (2) The histogram of the posterior relative frequency distribution of the damage index under different working conditions has obvious normal distribution characteristics, and the damage of the member itself and the neighboring members can be more obviously reflected

- in the change of the mean value of the Markov chain. And the mean value of the Markov chain of working conditions with a higher degree of damage tends to have greater changes, and when the member is completely cut, its own damage index will be close to 0.
- (3) The damage of the member itself and the neighboring members also have a significant impact on the damage probability, which is reflected in the fact that the higher the degree of damage, the higher the probability of damage tends to be. However, the diagnosis index is more sensitive to the damage of the member itself.
- (4) Compared with general statistical method and GMM clustering method, this method considers the uncertainty and effectively identifies cases that cannot be identified in other methods.
- (5) During the construction of the BDIA hanger roof, the structural lifting may cause changes in the boundary conditions and consequently in the structural state. Based on the field monitoring data of the BDIA hanger roof construction, after discussing the method of baseline state selection, the method proposed in this paper is used to effectively diagnose the structural state changes that could not be directly observed from the time history curves of strain and temperature.

Fig. 22 The Schematic diagrams of the hangar roof structure at BDIA and its sensor layout

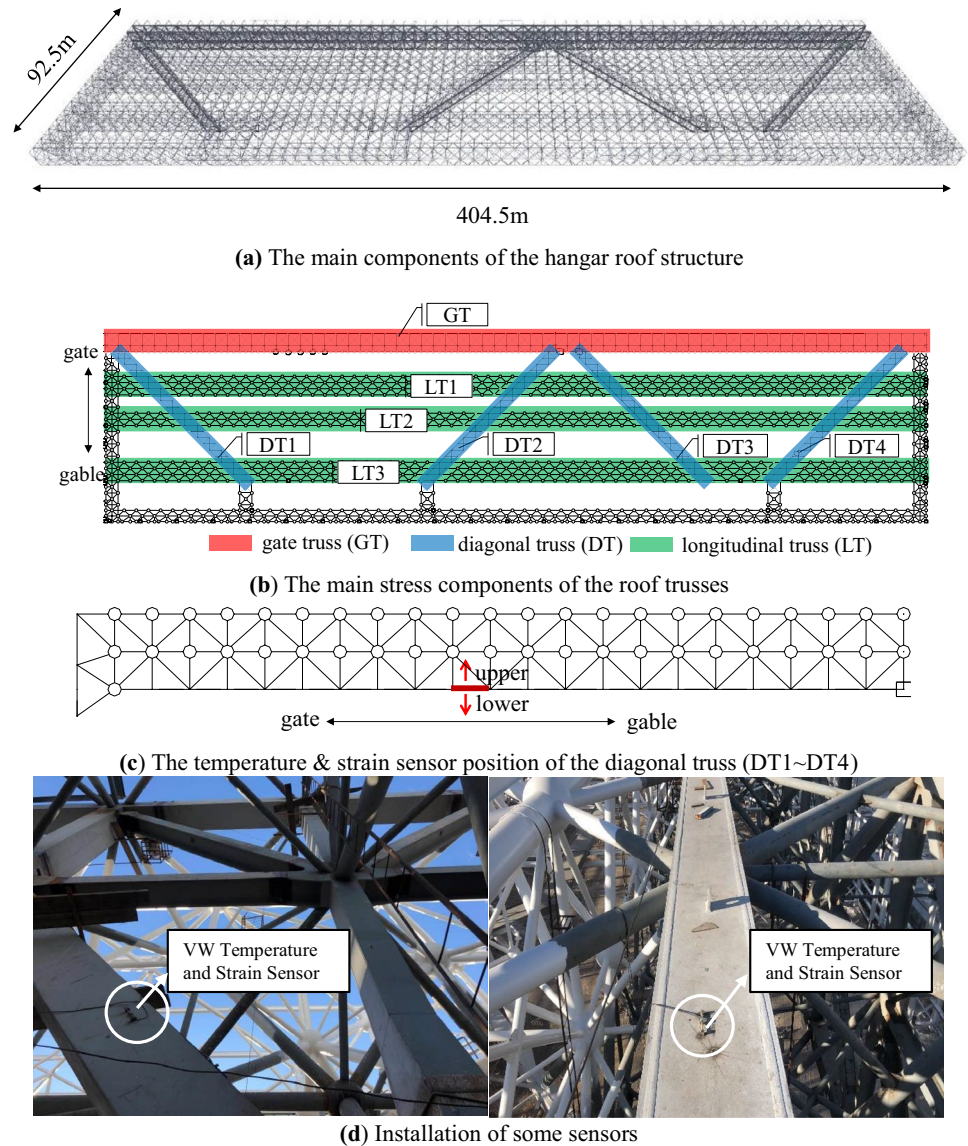


Table 9 Value of ADF test parameters

ADF test parameters	Value
Mean value	-1.6391
Standard deviation	0.2732
Test statistic	-5.6062
Critical value	-1.9416

Although the proposed method shows promising results, further research on diagnosis methods is needed, which will include the combination with other SAD methods as well as studying the application of the method to more forms of large-span spatial structures. Further work will also focus on more precise localization of the anomaly members and a more accurate reflection of the degree of anomaly.

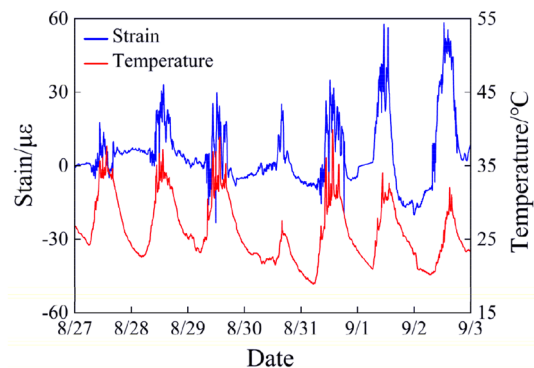


Fig. 23 Temperature and strain time history curves of the hangar roof structure (DT4-upper)

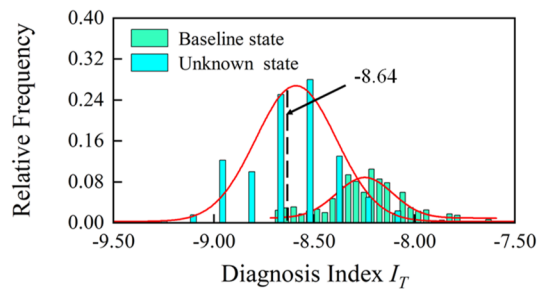


Fig. 24 Histogram of Markov chain relative frequency distribution of diagnosis index under baseline state and unknown state

Acknowledgements The authors would like to thank the support from The Joint Funds of the National Natural Science Foundation of China (U1939208), National Natural Science Foundation of China (No. 51525803) and the 111 Project (B20039).

References

- Xue SD (2020) Recent development and engineering practice of spatial structures in China. *Steel Constr (Chinese & English)* 35(7):1–16. <https://doi.org/10.13206/jgjsSE20041904>
- Sun H, Di S, Du Z et al (2021) Application of multisynchrosqueezing transform for structural modal parameter identification. *J Civ Struct Health Monit* 11:1175–1188. <https://doi.org/10.1007/s13349-021-00500-0>
- Ye X, Huang P, Pan C et al (2021) Innovative stabilization diagram for automated structural modal identification based on ERA and hierarchical cluster analysis. *J Civ Struct Health Monit* 11:1355–1373. <https://doi.org/10.1007/s13349-021-00514-8>
- Sunca F, Ergin M, Altunışik AC et al (2021) Modal identification and fatigue behavior of Eynel steel arch highway bridge with calibrated models. *J Civ Struct Health Monit* 11:1337–1354. <https://doi.org/10.1007/s13349-021-00512-w>
- Lorenzoni F, De Conto N, da Porto F et al (2019) Ambient and free-vibration tests to improve the quantification and estimation of modal parameters in existing bridges. *J Civ Struct Health Monit* 9:617–637. <https://doi.org/10.1007/s13349-019-00357-4>
- Cao J, Zhang S, Liu Y (2021) Probabilistic SDDL method for localizing damage in bridges monitored within one cluster under time-varying environmental temperatures. *J Civ Struct Health Monit*. <https://doi.org/10.1007/s13349-021-00524-6>
- Sarmadi H, Entezami A, Salar M (2021) Bridge health monitoring in environmental variability by new clustering and threshold estimation methods. *J Civ Struct Health Monit* 11:629–644. <https://doi.org/10.1007/s13349-021-00472-1>
- Sadhu A, Goli G (2017) Blind source separation-based optimum sensor placement strategy for structures. *J Civ Struct Health Monit* 7:445–458. <https://doi.org/10.1007/s13349-017-0235-6>
- João PS, Cremona C, André D et al (2015) Static-based early-damage detection using symbolic data analysis and unsupervised learning methods. *Front Struct Civ Eng* 9(1):1–16. <https://doi.org/10.1007/s11709-014-0277-3>
- Eun HC, Park SY, Lee MS (2013) Static-based damage detection using measured strain and deflection data. *Appl Mech Mater* 256–259:1097–1100. <https://doi.org/10.1007/s11709-014-0277-3>
- El-Sisi AEDA, El-Husseiny OM, Matar EB et al (2020) Field-testing and numerical simulation of vantage steel bridge. *J Civ Struct Health Monit* 10:443–456. <https://doi.org/10.1007/s13349-020-00396-2>
- Cocking S, Alexakis H, DeJong M (2021) Distributed dynamic fibre-optic strain monitoring of the behaviour of a skewed masonry arch railway bridge. *J Civ Struct Health Monit* 11:989–1012. <https://doi.org/10.1007/s13349-021-00493-w>
- Sun F, Hoult NA, Butler LJ et al (2021) Distributed monitoring of rail lateral buckling under axial loading. *J Civ Struct Health Monit*. <https://doi.org/10.1007/s13349-021-00504-w>
- Han QH, Ma Q, Xu J et al (2021) Structural health monitoring research under varying temperature condition: a review. *J Civ Struct Health Monit* 11:149–173. <https://doi.org/10.1007/s13349-020-00444-x>
- Duan YF, Li Y, Xiang YQ (2011) Strain-temperature correlation analysis of a tied arch bridge using monitoring data. In: 2011 international conference on multimedia technology. IEEE, Piscataway, pp 6025–6028. <https://doi.org/10.1109/ICMT.2011.6002979>
- Alexakis H, Lau FDH, DeJong MJ (2021) Fibre optic sensing of ageing railway infrastructure enhanced with statistical shape analysis. *J Civ Struct Health Monit* 11:49–67. <https://doi.org/10.1007/s13349-020-00437-w>
- Ding Y, Li AQ (2011) Assessment of bridge expansion joints using long-term displacement measurement under changing environmental conditions. *Front Struct Civ Eng* 5(3):37–380. <https://doi.org/10.1007/s11709-011-0122-x>
- Baraccani S, Palermo M, Gasparini G (2021) A time domain approach for data interpretation from long-term static monitoring of historical structures. *Struct Control Health Monit* 28:e2708. <https://doi.org/10.1002/stc.2708>
- Xia Q, Zhou LM, Zhang J (2018) Thermal performance analysis of a long-span suspension bridge with long-term monitoring data. *J Civ Struct Health Monit* 8:543–553. <https://doi.org/10.1007/s13349-018-0299-y>
- Xia Q, Zhang J, Tian YD (2017) Experimental study of thermal effects on a long-span suspension bridge. *J Bridge Eng* 22(7):4017034. [https://doi.org/10.1061/\(ASCE\)BE.1943-5592.0001083](https://doi.org/10.1061/(ASCE)BE.1943-5592.0001083)
- Kulprapha N, Warnitchai P (2012) Structural health monitoring of continuous prestressed concrete bridges using ambient thermal responses. *Eng Struct* 40:20–38. <https://doi.org/10.1016/j.engstruct.2012.02.001>
- Yarnold MT (2013) Temperature-based structural identification and health monitoring for long-span bridges. Dissertation, Drexel University.
- Yarnold MT, Franklin LM, Aktan AE (2015) Temperature-based structural identification of long-span bridges. *J Struct Eng* 141(11):04015027. [https://doi.org/10.1061/\(ASCE\)ST.1943-541X.0001270](https://doi.org/10.1061/(ASCE)ST.1943-541X.0001270)
- Yarnold MT, Fl M (2015) Temperature-based structural health monitoring baseline for long-span bridges. *Eng Struct* 86:157–167. <https://doi.org/10.1016/j.engstruct.2014.12.042>
- Murphy B, Yarnold MT (2018) Temperature-driven structural identification of a steel girder bridge with an integral abutment. *Eng Struct* 155:209–221. <https://doi.org/10.1016/j.engstruct.2017.10.074>
- Lyu M, Zhu X, Yang Q (2017) Connection stiffness identification of historic timber buildings using temperature-based sensitivity analysis. *Eng Struct* 131:180–191. <https://doi.org/10.1016/j.engstruct.2016.11.012>
- Kromanis R, Kripakaran P (2014) Predicting thermal response of bridges using regression models derived from measurement histories. *Comput Struct* 136(2014):64–77. <https://doi.org/10.1016/j.compstruc.2014.01.026>

28. Kromanis R (2015) Structural performance evaluation of bridges: characterizing and integrating thermal response. Dissertation, University of Exeter
29. Kromanis R, Kripakaran P (2016) SHM of bridges: characterising thermal response and detecting anomaly events using a temperature-based measurement interpretation approach. *J Civ Struct Health Monit* 6(2):237–254. <https://doi.org/10.1007/s13349-016-0161-z>
30. Kromanis R, Kripakaran P (2021) Performance of signal processing techniques for anomaly detection using a temperature-based measurement interpretation approach. *J Civ Struct Health Monit* 11:15–34. <https://doi.org/10.1007/s13349-020-00435-y>
31. Xia Q, Cheng YY, Zhang J et al (2016) In-service condition assessment of a long-span suspension bridge using temperature-induced strain data. *J Bridge Eng* 22(3):4016124. [https://doi.org/10.1061/\(ASCE\)BE.1943-5592.0001003](https://doi.org/10.1061/(ASCE)BE.1943-5592.0001003)
32. Diao Y, Sui Z, Guo K (2021) Structural damage identification under variable environmental/operational conditions based on singular spectrum analysis and statistical control chart. *Struct Control Health Monit* 28:e2721. <https://doi.org/10.1002/stc.2721>
33. Tu JQ, Tang ZF, Yun CB (2021) Guided wave-based damage assessment on welded steel I-beam under ambient temperature variations. *Struct Control Health Monit* 28:e2696. <https://doi.org/10.1002/stc.2696>
34. Chen DS, Xu WC, Qian HL et al (2020) Effects of non-uniform temperature on closure construction of spatial truss structure. *J Build Eng*. <https://doi.org/10.1016/j.jobbe.2020.101532>
35. Xu WC, Chen DS, Qian HL et al (2021) Non-uniform temperature field and effects of large-span spatial truss structure under construction: field monitoring and numerical analysis. *Struct* 29:416–426. <https://doi.org/10.1016/j.istruc.2020.11.014>
36. Zhou M, Fan JS, Liu YF et al (2020) Non-uniform temperature field and effect on construction of large-span steel structures. *Automat Constr* 119:103339. <https://doi.org/10.1016/j.autcon.2020.103339>
37. Zhou M, Fan JS, Liu YF et al (2020) Analysis on non-uniform temperature field of steel grids of Beijing Daxing international airport terminal building core area considering solar radiation. *Eng Mech* 37(5):46–54/73. <https://doi.org/10.6052/j.issn.1000-4750.2019.07.0374> (in Chinese)
38. Luo YZ, Mei YJ, Shen YB et al (2013) Measurement and analysis of steel structure temperature and stress in National Stadium. *J Build Struct* 34(11):24–32. <https://doi.org/10.14006/j.jzjgxb.2013.11.005> (in Chinese)
39. Hu YD, Hou RR, Xia Q et al (2018) Temperature-induced displacement of supertall structures: a case study. *Adv Struct Eng* 22(4):982–996. <https://doi.org/10.1177/1369433218795288>
40. Sohn H, Dzwonczyk M, Straser EG et al (1999) An experimental study of temperature effect on modal parameters of the Alamosa Canyon Bridge. *Earthq Eng Struct Dyn* 28(8):879–897. [https://doi.org/10.1002/\(sici\)1096-9845\(199908\)28:8%3c879::aid-eqe845%3e3.0.co;2-v](https://doi.org/10.1002/(sici)1096-9845(199908)28:8%3c879::aid-eqe845%3e3.0.co;2-v)
41. Xia Q, Tian YD, Cai DX (2020) Structural flexibility identification and fast-Bayesian-based uncertainty quantification of a cable-stayed bridge. *Eng Struct* 214:110616-1-110616–11. <https://doi.org/10.1016/j.engstruct.2020.110616>
42. Xu M, Guo J, Wang S (2021) Structural damage identification with limited modal measurements and ultra-pars Bayesian regression. *Struct Control Health Monit* 28:e2729. <https://doi.org/10.1002/stc.2729>
43. Wang YW, Ni YQ, Zhang QH (2021) Bayesian approaches for evaluating wind-resistant performance of long-span bridges using structural health monitoring data. *Struct Control Health Monit* 28:e2699. <https://doi.org/10.1002/stc.2699>
44. Wang XY, Hou R, Xia Y et al (2020) Laplace approximation in sparse Bayesian learning for structural damage detection. *Mech Syst Signal Pr* 140:106701. <https://doi.org/10.1016/j.ymsp.2020.106701>
45. Wang XY, Li L, Beck JL et al (2021) Sparse Bayesian factor analysis for structural damage detection under unknown environmental conditions. *Mech Syst Signal Pr* 154(11):107563. <https://doi.org/10.1016/j.ymsp.2020.107563>
46. Hou R, Wang XY, Xia Q et al (2020) Sparse Bayesian learning for structural damage detection under varying temperature conditions. *Mech Syst Signal Pr* 145:106965. <https://doi.org/10.1016/j.ymsp.2020.106965>
47. Wang X, Hou R, Xia Y et al (2020) Structural damage detection based on variational Bayesian inference and delayed rejection adaptive Metropolis algorithm. *Struct Health Monit* 20(4):147592172092125. <https://doi.org/10.1177/147592172092125>
48. Huang T, Schroeder KU (2020) Bayesian probabilistic damage characterization based on a perturbation model using responses at vibration nodes. *Mech Syst Signal Pr* 139:106444. <https://doi.org/10.1016/j.ymsp.2019.106444>
49. Huang T, Schrder KU (2021) IWSHM 2019: Perturbation-based Bayesian damage identification using responses at vibration nodes. *Struct Health Monit* 20(3):942–959. <https://doi.org/10.1177/1475921720985143>
50. Alkam F, Lahmer T (2021) Eigenfrequency-based Bayesian approach for damage identification in catenary poles. *Infrastruct*. <https://doi.org/10.3390/infrastructures6040057>
51. Cantero-Chinchilla S, Malik MK, Chronopoulos D et al (2021) Bayesian damage localization and identification based on a transient wave propagation model for composite beam structures. *Compos Struct* 267:113849. <https://doi.org/10.1016/j.compstruct.2021.113849>
52. Barron RF, Barron BR (2011) Design for thermal stresses. Wiley, New Jersey. <https://doi.org/10.1002/9781118093184:416-460>
53. Price R (2003) An essay towards solving a problem in the doctrine of chances. *Resonance* 8(4):80–88. <https://doi.org/10.1007/10.1007/BF02883540>
54. Hastings WK (1970) Monte Carlo sampling methods using Markov chains and their applications. *Biometrika* 57(1):97–109. <https://doi.org/10.2307/2334940>
55. Metropolis N, Rosenbluth AW, Rosenbluth MN (1953) Equation of state calculations by fast computing machines. *J Chem Phys* 1(6):1087–1092. <https://doi.org/10.1063/1.1699114>
56. Dutta A, McKay M, Kopsaftopoulos F et al (2021) Statistical residual-based time series methods for multicopter fault detection and identification. *Aerosp Sci Technol* 112(1):106649. <https://doi.org/10.1016/j.ast.2021.106649>
57. Sarmadi H, Yuen KV (2020) Early damage detection by an innovative unsupervised learning method based on kernel null space and peak-over-threshold. *Comput-Aided Civ Inf* 36(9):1150–1167. <https://doi.org/10.1111/mice.12635>
58. Vidya SR (2018) Verification of the applicability of the Gaussian mixture modelling for damage identification in reinforced concrete structures using acoustic emission testing. *J Civ Struct Health Monit* 8:395–415. <https://doi.org/10.1007/s13349-018-0284-5>
59. Said SE, Dickey DA (1984) Testing for unit roots in autoregressive-moving average models of unknown order. *Biometrika* 3:599–607. <https://doi.org/10.2307/2336570>

Publisher's Note Springer Nature remains neutral with regard to jurisdictional claims in published maps and institutional affiliations.